

# Modelling the Sun as an active star

## I. A diagnosis of photometric starspot models

K. Oláh<sup>1</sup>, L. van Driel-Gesztelyi<sup>1,2</sup>, Zs. Kővári<sup>1</sup>, and J. Bartus<sup>1</sup>

<sup>1</sup> Konkoly Observatory of the Hungarian Academy of Sciences, H-1525 Budapest, Hungary (olah; kovari; bartus@buda.konkoly.hu)

<sup>2</sup> Observatoire de Paris, DASOP, F-92195 Meudon Cedex, France (lvandrie@mesioq.obspm.fr)

Received 4 November 1998 / Accepted 4 January 1999

**Abstract.** We provide a diagnosis of photometric starspot models through modelling active areas on the Sun using softwares originally written for starspot modelling. The data we used were one-dimensional measurements of the Sun in radio (10.7 cm, DRAO, Canada) and in soft X-rays (GOES satellites). In these wavelengths the response to magnetic activity results in similar amplitude variability on the Sun to those we attribute to starspots in visual wavelengths. The modelling results were compared with contemporaneous direct images (obtained at Nobeyama, Japan and with the Yohkoh and SOHO spacecraft).

We found that: *a*) knowing well the basic physical parameters of a star, the resulting total spotted area is a fairly good approximation of the reality, thus making sense of photometric starspot modelling; *b*) long-term variability coupled with the rotational modulation may result in artificially high latitude spots; *c*) in two- or multi-spot models a resulting small spot can account for short living spots; *d*) systematic change in spot size could be partially due to flux ratio changes. The contrast between the studied bright active region and the undisturbed area on the Sun decreased in time following roughly a power law. At the same time, the emission measure of the active region's core similarly decreased.

**Key words:** Sun: activity – Sun: radio radiation – Sun: X-rays, gamma rays – stars: activity – stars: imaging – stars: starspots

### 1. Introduction

Already in the mid-seventies, when the stellar activity studies began, methods were developed to model the light variability of spotted stars (cf. Bopp & Evans 1973, Budding 1977). Since that time, it was also clear that solutions of the inverse problem, which use one-dimensional data to recover two-dimensional surface distribution on stellar surfaces, have serious stability and non-uniqueness problems. A few attempts have already been made to study these questions (see e.g. Kővári & Bartus 1997). However, the best test one can imagine would be just to compare the modelling result with the direct image of an active star.

The possibility for making this test has been formed in the recent years, using the Sun as an active star. The first attempt for this experiment was made by Catalano et al. (1998). They compared the chromospheric map of the Sun obtained from the deconvolution of the C II line flux at 133.5nm with the direct H $\alpha$  images for about 10 solar rotations in 1992–93. The agreement between the modelled maps and the direct images were very good: only low contrast ( $\Delta I/I < 0.3$ ) and small ( $< 20^\circ - 30^\circ$  in diameter) features were missing. The solar observations were made in the equatorial plane, so there was no latitude information in the derived maps.

Another method to study the solar-stellar connections was presented by Peres et al. (1998). They used Yohkoh/SXT images of the Sun to synthesize solar spectra similar to those gathered for stars by ROSAT/PSPC and ASCA/SIS. The spectra made at quiet and active states of the Sun were well fitted by standard stellar one- and two-thermal-component models, respectively.

In mid-1996, at its activity minimum, the Sun had only one major active region (NOAA AR 7978) beside some small, short-lived ones. The big active region (AR afterwards) emerged between 6–9 July, 1996 and it dominated the solar activity, while decaying, for four more rotations (Hudson et al. 1997, Harvey & Hudson 1997, van Driel-Gesztelyi 1998). During this time, daily direct images were obtained in several wavelengths, and, at the same time, one-dimensional ground-based and satellite data were gathered with detectors that measured the Sun as a star.

The Sun is a slowly rotating ( $P_{rot} \approx 27^d.25$ ) G2V single star. Rotational modulation caused by ARs is observed in several wavelengths from the photosphere through the chromosphere to the corona. Sunspots themselves cause only a very small amplitude light variation as the Sun rotates, much smaller than we observe on stars as rotational modulation.

However, in the second half of 1996, the amplitude of the solar variability in the 10.7 cm radio wavelength was similar to a typical stellar rotational modulation in the optical domain. At the same time, the solar X-ray amplitude was a few times higher, but still comparable to the stellar ones. The available images and contemporaneous one-dimensional observations of the Sun at its activity minimum with only one major AR thus made it possible to model the Sun as a star, and to compare the

**Table 1.** 10.7 cm radio (DRAO, Canada), soft X-ray (GOES9 satellite) and Yohkoh results used in the modelling

date	J.D.	area <sup>a</sup>	$I_{\text{rad}}$	$I_{\text{rad}}/I_{0,\text{rad}}$ <sup>b</sup>	$E_{\text{rad}}$ <sup>c</sup>	$I_{\text{X}}$	$I_{\text{X}}/I_{0,\text{X}}$ <sup>d</sup>	$E_{\text{X}}$ <sup>e</sup>	EM/pixel <sup>f</sup>	EM <sup>g</sup>
1996	2400000+	( $A_{\text{spot}}$ )	Jansky			$\text{Wm}^{-2}$			central part	
7 July	50272	0.019	$75.0 \cdot 10^4$	1.11	59	$0.39 \cdot 10^{-7}$	9.8	513	7.0	5.6
10 July	50275	0.020	$83.4 \cdot 10^4$	1.24	62	$2.28 \cdot 10^{-7}$	57.0	2850	19.0	15.2
2 Aug	50298	0.035	$81.5 \cdot 10^4$	1.22	35	$0.93 \cdot 10^{-7}$	23.3	664	8.3	6.6
30 Aug	50326	0.042	$74.7 \cdot 10^4$	1.11	27	$0.58 \cdot 10^{-7}$	14.5	345	5.9	4.7
25 Sep	50352	0.051	$71.2 \cdot 10^4$	1.06	21	$0.23 \cdot 10^{-7}$	5.8	113	1.8	1.4
23 Oct	50380	0.072	$69.6 \cdot 10^4$	1.04	14	$0.09 \cdot 10^{-7}$	2.3	31	1.3	1.0
18 Nov	50406	0.079	$72.6 \cdot 10^4$	1.08	14	$0.12 \cdot 10^{-7}$	3.0	38	0.4	0.3

<sup>a</sup> the visible solar disk ( $A_{\text{disc}} = 1$ ); <sup>b</sup>  $I_{0,\text{rad}} = 67 \cdot 10^4 \text{ Jansky} = 67 \cdot 10^{-22} \text{ Wm}^{-2} \text{ Hz}^{-1}$ ; <sup>c</sup>  $E_{\text{rad}} = \text{radio emissivity}$

<sup>d</sup>  $I_{0,\text{X}} = 0.04 \cdot 10^{-7} \text{ Wm}^{-2}$ ; <sup>e</sup>  $E_{\text{X}} = \text{X-ray emissivity}$ ; <sup>f</sup>  $\times 10^{44}$  pixel (with  $4''.91 \times 4''.91$  pixel size); <sup>g</sup>  $\times 10^{27} \text{ cm}^{-5}$

results with the direct images. However, during the modelling we treated the one dimensional data (the light curves) as the only information.

## 2. Data

For the analysis we used two one-dimensional datasets: radio and soft X-ray data. The solar images we compared to the modelling results were obtained with the Yohkoh spacecraft.

Daily 10.7 cm radio solar flux measurements are recorded at the Dominion Radio Astrophysical Observatory (DRAO) at Penticton, Canada (Tapping & Charrois 1994). The daily flux is measured at 18:00, 20:00, and 22:00 UT from November, 1995 through February, 1996, and at 17:00, 20:00, and 23:00 UT from March, 1996 through October, 1996. The data is given in solar flux units ( $10^{-22} \text{ Wm}^{-2} \text{ Hz}^{-1}$ ) or  $10^4$  Janskys.

Geostationary Orbiting Environmental Satellites (GOES) provide soft X-ray irradiance measurements in the 1–8 Å flux range in  $\text{Wm}^{-2}$ . For our analysis we use data from the GOES9 satellite. Note that both the DRAO and GOES measurements were calibrated to 1 AU distance.

We make use of full-disc images recorded with the grazing incidence soft X-ray telescope (SXT) instrument onboard Yohkoh. The SXT has been described in detail by Tsuneta et al. (1991). It is sensitive to X-rays in the energy range 0.25–4.0 keV.

As an illustration, we used one Nobeyama radio image. Full-disc radio images are taken with the Nobeyama Radioheliograph at 17GHz ( $\lambda = 1.7635 \text{ cm}$ ). The instrument is a radio interferometer, which consists of eighty-four 80 cm diameter antennas arranged in a ‘T’-shaped array. The spatial resolution is  $10''$  (Nishio et al. 1994, Hanaoka et al. 1994).

MDI (Michelson Doppler Imager) is one of the twelve experiments onboard SOHO, which measures the photospheric manifestation of solar oscillation (Scherrer et al. 1995). Besides the dopplergrams it records the line-of-sight magnetic field with a resolution of  $2''$  in the full-disc mode we use.

In this study, SOHO/EIT (Extreme Ultraviolet Imaging Telescope, Delaboudinière et al. 1995) He II 304 Å images were also used for illustration.

In Table 1 we present area and intensity measurements of NOAA AR 7978, near the time of its birth and at or close to its central meridian passages. Area measurements were made

on Yohkoh images, whereas radio and X-ray intensities ( $I_{\text{rad}}$ ,  $I_{\text{X}}$ ) were taken from DRAO and GOES data. The radio and X-ray emissions at the DRAO and GOES wavelengths come from the lower and higher solar corona, respectively. Therefore we can suspect that the areas where these emissions originate were similar to each other and to the AR area displayed by Yohkoh. The spatial correlation of the different layers of NOAA AR 7978 is well demonstrated by van Driel-Gesztelyi (1998). For the flux ratio calculations (Sect. 4.1.) thus we used only the Yohkoh areas. The undisturbed solar intensities ( $I_{0,\text{rad}}$ ,  $I_{0,\text{X}}$ ) in wavelengths of DRAO and GOES were measured at the 1996 sunspot minimum, that falls in the time interval of our study. We also calculated the emissivities ( $E_{\text{rad}}$ ,  $E_{\text{X}}$ ) that give the flux per unit area ratio of the emitting and the undisturbed solar surface. It is well seen from Table 1, that the emissivity of the AR, after the first few days, was continuously decreasing, leading to an unexpected problem in the data analysis, that we discuss later.

## 3. Method

The one-dimensional measurements of active stars (usually photometric, but also in other wavelength ranges as radio or X-rays) have a limited information content, therefore in the modelling procedure simplified assumptions are used. Usually two, sometimes three dark (or bright) areas are supposed to describe the light variability. Spot temperatures are derived from multicolour data, and homogeneous temperature distribution inside the spots is assumed. This temperature and the temperature of the immaculate star is used to derive the flux ratio between the stellar surface and the spot. The same, generally linear limb darkening function is used for the spot and the undisturbed surface. To keep the number of the free parameters as low as possible, the physical parameters of the stars (surface and spot temperatures, limb darkening, inclination) are kept fixed during the modelling, and only the spot coordinates and sizes are to be derived.

The solar radio and X-ray data were modelled using the software package TISMO (*T*/me-series *S*pot *M*Odelling, Bartus 1996) with a small modification (see Sect. 4.1. below). This code was originally developed to model photometric light curves of spotted stars aimed at determining the geometric parameters of stellar spots. The circular spot approach based on Budding’s equations (1977) was applied. The fitting was carried out with

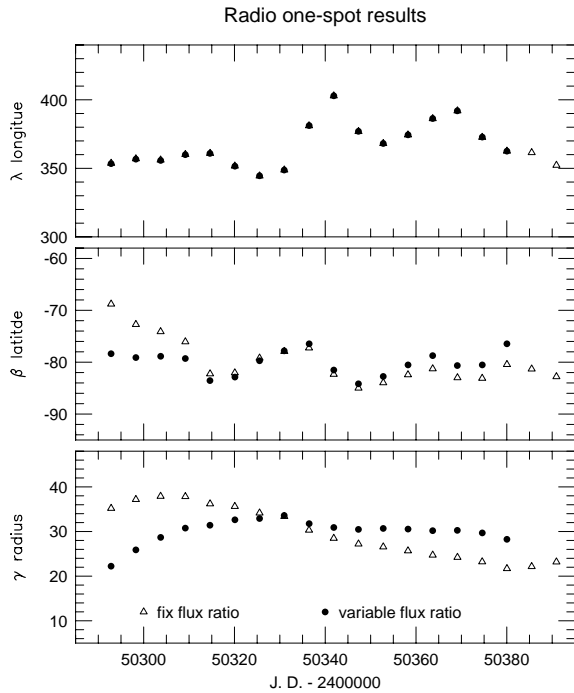


**Fig. 1.** Computed longitude, latitude and size of the spot on the Sun using one-spot approximations, with constant and variable flux ratios. See explanation in the text.

Levenberg-Marquardt method (Press et al., Numerical Recipes in C 1988).

TISMO walks along a time-series data in the following way: first it reads in a part of the dataset, of which length is given as an input value in units of photometric phase. From this amount of data the program forms a phased light curve and calculates the spot parameters. Then TISMO steps on in the dataset with a given time interval (that is also an input value in units of photometric phase). This procedure is repeated until the algorithm reaches the end of the datafile. TISMO thus allows to use any arbitrary segment of time-series data and is able to calculate time-series spot models with any given density. The code also allows to model observations in the form of single phased light curves using all the available data, of which length is calculated in units of photometric phase, and the length of the step is the same.

For modelling radio observations we used 1.2 cycles long datasets (i.e. overlapping rotations) with 0.2 steps of phase (that is  $\approx 5.5$  days), whereas for X-ray data, because of their much higher fluctuations, data of 0.7 cycles long (i.e. less than one rotation) was used, also with 0.2 steps of phase.

Micro- and macroflares that occurred very frequently especially in the first half of the modelled time interval, were removed from the GOES9 X-ray data. To get similar number of data in radio and X-rays, the GOES9 measurements were averaged forming 3 daily values. The physical parameters of the Sun were set up as follows: we used constant inclination of  $86^\circ$  (although during the modelled time-interval the inclination of the Sun changed a few degrees, but that change affects the

modelling results well within the error of the procedure). Phases were computed with the elements of J.D.  $50298.0 + 27^d.25 \times E$ , zero longitude is at the central meridian. Limb darkening value of  $-0.3$  was used in radio (Hachenberg 1982), and since the Sun is transparent in X-rays, we set the limb darkening to 0.0 in this wavelength. The unspotted intensities of the Sun were chosen to be 67 Jansky ( $67 \cdot 10^{-22} \text{Wm}^{-2} \text{Hz}^{-1}$ ) in radio and  $0.04 \cdot 10^{-7} \text{Wm}^{-2}$  in X-rays, as measured at the 1996 sunspot minimum. The flux ratio values we used are discussed in the next section in detail.

## 4. Results

### 4.1. Flux ratio changes

During the first few modelling runs we used constant flux ratios between the AR and the undisturbed surface of the Sun: 3.0 for radio, and 236 for X-rays. We calculated these values from average intensity ratios between the spot and the background given by the measurements, supposing an  $\approx 5\%$  spot area, typical for large ARs. Using constant flux ratios the resulting spot sizes were decreasing with the amplitude of the variation, as it is seen in Fig. 1. This result led us to cast a glance at the direct images to see what had happened. We had to notice that the sizes of the ARs had not been decreasing, but increasing. The only possible reason for this discrepancy is the change (i.e., the decrease) in the contrast term between the spot and the unspotted surface that affects strongly the spot size. Using a series of Yohkoh/SXT direct images and the GOES9 X-ray and DRAO radio fluxes, we calculated flux ratios ( $FR$ ) for the time of all consecutive meridian passages of the big AR from the following ratio:

$$\frac{I}{I_0} = \frac{FR \times A_{\text{spot}} + (A_{\text{disc}} - A_{\text{spot}})}{A_{\text{disc}}}, \quad (1)$$

where  $I$  and  $I_0$  were the spot and background intensities in radio and X-rays, and  $A_{\text{spot}}$  and  $A_{\text{disc}}$  were the areas of the AR and the solar disc; all these values are given in Table 1. Additionally, the emission measure ( $EM$ ) of the brightest central part of the AR in X-rays was derived from Yohkoh/SXT images, using the AlMg and Al12 filter ratio. The basic difference between the  $FR$  and the  $EM$  values is that the former is derived from one-dimensional data, supposing homogeneous bright spot area and an immaculate background (which is not strictly true), while the  $EM$  measurements were carried out in 2D images, where the AR was surrounded by a contour, excluding the changing background.

Both the  $FR$  and the  $EM$  decrease follow a power law (a hyperbola):

$$FR(J.D.) \text{ or } EM(J.D.) = c_1 + \frac{c_2}{(J.D. - J.D.(0))^{c_3}}, \quad (2)$$

where  $J.D.(0)$  is the approximate Julian Date of the emergence of the AR,  $c_1$  is the asymptotic value where  $FR$  or  $EM$  tends to, that equals 1 for  $FR$  and the emission measure of the background for  $EM$ ,  $c_2$  is a constant resulting from least-squares fits, and  $c_3$  is the parameter that describes the speed of the decrease. In the first two panels of Fig. 2 we plot the fitted  $FR$  change in

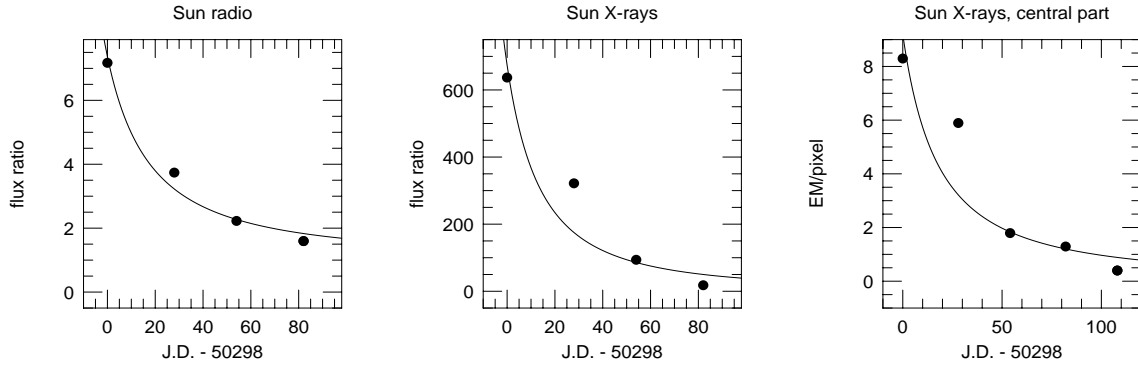


**Fig. 2.** Flux ratio ( $FR$ ) changes between the AR and the undisturbed solar surface computed from one dimensional data in radio and X-ray wavelengths, and X-ray emission measure evolution in the central part of the AR measured on Yohkoh images.

radio and X-ray wavelengths, while the third panel shows the  $EM$  evolution. For  $c_3$  we got fairly similar values: 1.4, 1.8 and 1.4 for the radio, the X-rays, and the X-ray  $EM$  of the central part, respectively. Around the time of the last analysed meridian passage of the big AR in November, a few new ARs appeared in the vicinity of the decaying AR, so the one-dimensional measurements did not correspond to one single AR, therefore the  $FR$  changes could not be followed anymore.

Consequently, we modified our modelling program to take the variability of the flux ratio into account in the form given in Eq. 2, not forgetting that the reality is more complicated.

#### 4.2. Modelling results

Fig. 3 shows the fitted radio and X-ray data. The light curves are quasi-sinusoidal, meaning that one active area dominates, therefore a one-spot model can give fairly acceptable fit. This is true especially for the second half of the observational period. During the first two rotations the deviation from the pure sinusoidal wave of the light curves were caused by an additional spot. In the course of the two-spot modelling first we fixed the spots to the equator, since the latitude is usually the most unstable spot parameter in the modelling, especially at such a high inclination as is our case. In the third run the spot coordinates and sizes were all free parameters. The resulting spot parameters are displayed in Fig. 4a, 4b and 4c. In Table 2 we present similar modelling results, which were computed individually for the four rotations of the observations. These resulting parameters fit well the corresponding time-series results in Fig. 4a, 4b and 4c.

In this study, the uncertainty of the parameter determination, in the case of the main spot is about  $10^\circ - 15^\circ$  in longitude,  $\approx 5^\circ$  in latitude and  $1^\circ - 3^\circ$  in spot radius. The very high latitude of the main spot makes the longitude value unstable. For the second, small spot only the longitude value has some reality with its  $25^\circ - 40^\circ$  error, the latitude is not determinable, and (as partly a consequence of this) the radius determination has an error of  $10^\circ - 15^\circ$ , comparable to the resulting spot sizes. Thus, although the light curves suggest the existence of at least one additional spot, its parameters cannot really be recovered. Nevertheless, the resulting spot parameters in radio and X-ray wavelengths are in good agreement (see Fig. 4a, 4b and 4c), and also, the

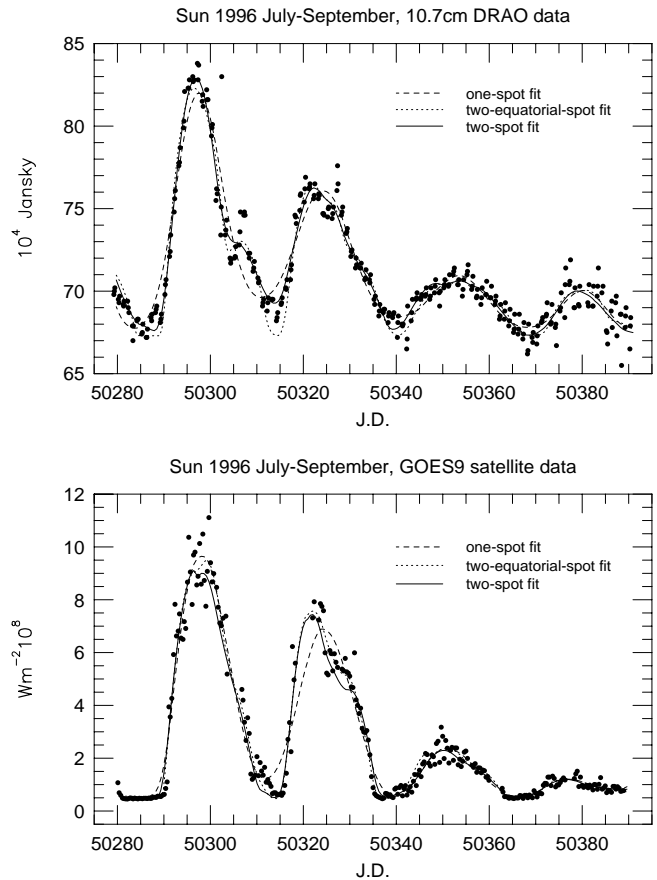


**Fig. 3.** Modelled radio (*top*) and X-ray (*bottom*) variability of the Sun.

derived total spotted area (3% – 6% of the solar surface) agrees very well with the directly measured values from the images (3% – 5% of the solar surface).

Test modelling showed, that if we suppose three spots for any of the data segments, the results became totally unstable because of the followings: *a*) relatively high scatter of the data (5%–10% of the amplitude), *b*) nine free parameters (six coordinates and three sizes), and *c*) high inclination. Only the big AR could be recovered within acceptable limits. Earlier modelling results showed, that only in an exceptional case of a light curve of

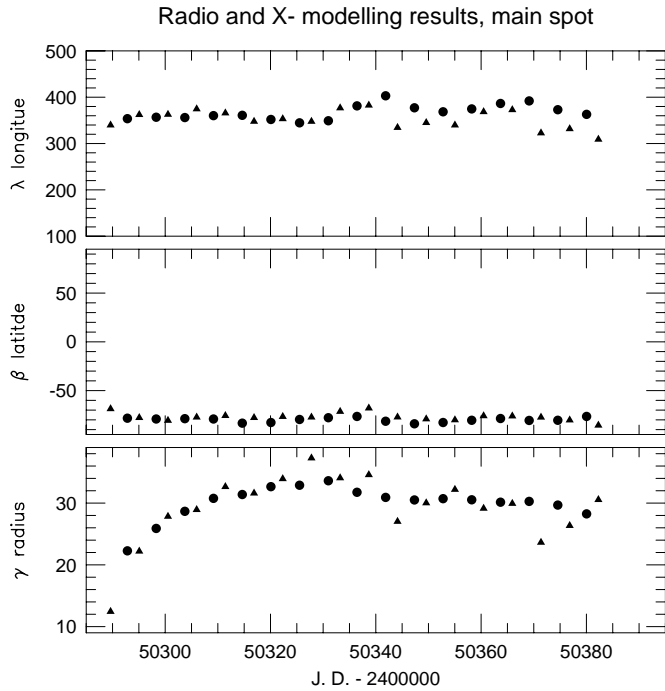


**Fig. 4a.** Computed longitude, latitude and size of the spot on the Sun using one-spot fit. Dots and triangles represent determinations from radio and X-ray data.

very high amplitude and excellent accuracy, was possible to recover three spots on a stellar surface (XX Tri) confirmed by two different modelling methods (Strassmeier & Oláh 1992).

## 5. Discussion

### 5.1. The reliability of starspot modelling in the view of our experiment

The reliability of our modelling was tested comparing the results with direct images of the Sun. In Fig. 5a, 5b and 5c the solar Yohkoh/SXT images on 1 September, 1996 (=J.D. 50328) are seen, together with the corresponding interpolated spot modelling results (see Fig. 4a, 4b and 4c). This day the two ARs were both well visible on the same hemisphere.

Figs. 5a and 5c show that the calculated latitude of the main spot is close to the pole. This is explained in the following way: during the second solar rotation of the investigated interval, a small, short lived AR had appeared on the Sun on 14 August 1996 (=J.D. 50310), when none of the two suspected ARs had been in view, therefore the radiated flux did not fall back to the unspotted level measured at the solar minimum later in mid-October, around J.D. 50370 (fourth minimum in the light curve). The modelling program thus artificially placed the main spot close to the polar region, to shift a part of it to the other hemisphere, accounting for the extra radiation originated from that side. This is well seen in Fig. 6, where Yohkoh/SXT images of the Sun are displayed, during central meridian passages of the main AR (light maximum, right column), and about half a rotation earlier (light minimum, left column).

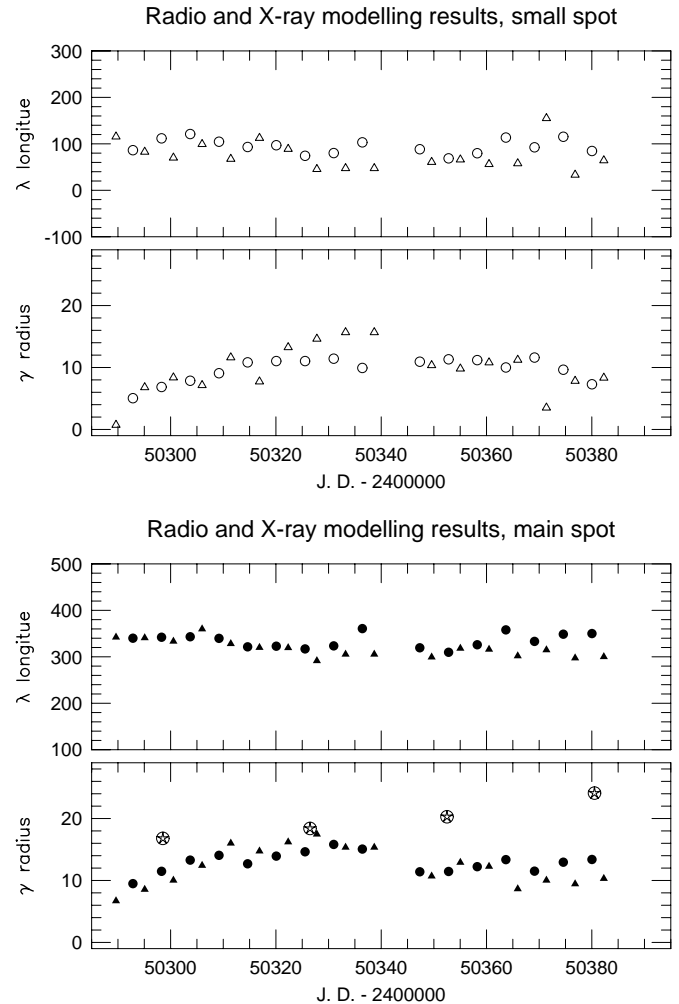


**Fig. 4b.** As in Fig. 4a, for two-equatorial-spot fit, latitude values were set to 0. Circled asterisks in the lowest panel display the size of the main spot measured from direct images at or close to the central meridian passage of the spot.

The real spot configuration was best approximated by two-equatorial-spots. This approach could not fully account for the extra radiation caused by the small, short lived spot on the other hemisphere (see Fig. 6), so the fit deviates somewhat from the observations at the first three minima (see Fig. 3). For the same reason (the small short-lived spot on the other hemisphere) the modelled size of the main spot was smaller, and of the small spot was bigger, and the longitude difference between the spots is close to the limb all the time, trying to account for the extra radiation originating from the other hemisphere.

The second spot, which, in fact, disappeared after not more than two rotations, was used for the fit during the whole time-interval. The code, thus, could fit the minima that were never flat, with an AR moved into, or out of view during all the modelling. Fig. 7 gives an example of this feature. The Yohkoh/SXT as well as the Nobeyama radio images made on 24 August, 1996 (=J.D. 50320) show two small, new ARs beside the main AR, and one of those is just at the western (right) limb of the Sun. Another

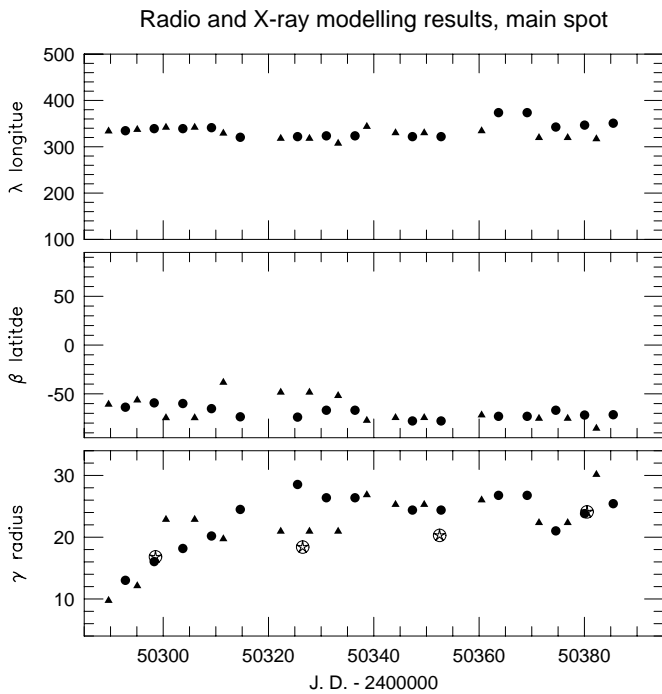
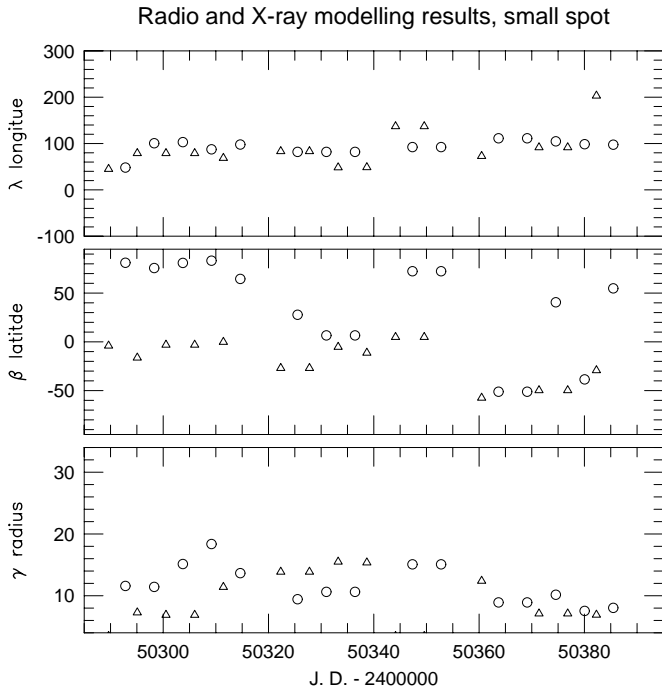


**Fig. 4c.** As in Fig. 4a, for two-spot fit, spot coordinates and sizes were all free parameters. Circled asterisks in the lowest panel display the size of the main spot measured from direct images at or close to the central meridian passage of the spot.

point of importance of Fig. 7 is, that the 17 GHz radio emission originates fairly close to the solar surface, whereas in X-rays the AR seem to have a considerable vertical extent. However, even in X-rays, most of the radiation comes from a relatively thin layer as shown by Hudson et al. (1997).

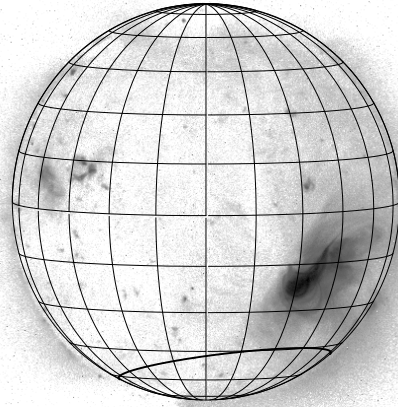


**Fig. 5a.** Yohkoh/SXT negative image of the Sun on 1 September, 1996 (J.D. 2450328), and the one-spot modelling result interpolated for the same day (see Fig. 4a.)

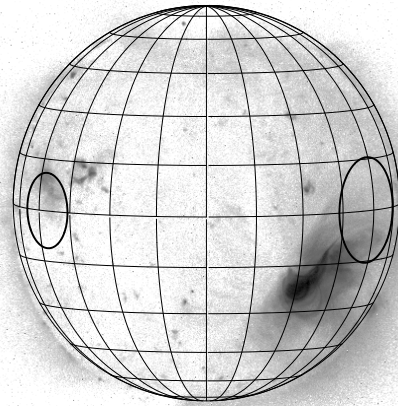


**Fig. 5b.** Yohkoh/SXT negative image of the Sun on 1 September, 1996 (J.D. 2450328), and the two-equatorial-spot modelling result interpolated for the same day (see Fig. 4b.)

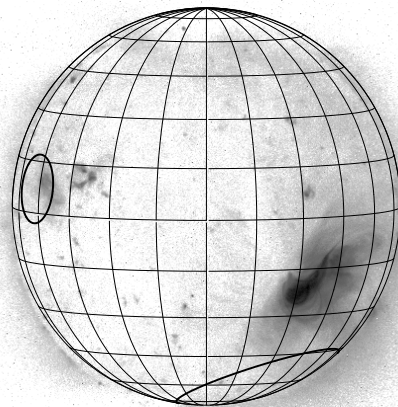


**Fig. 5c.** Yohkoh/SXT negative image of the Sun on 1 September, 1996 (J.D. 2450328), and the two-spot modelling result interpolated for the same day (see Fig. 4c.)

**Table 2.** Individual modelling results for the four observed rotations

rotation		1. spot			2. spot		
$\overline{J.D.}$		$\lambda_1$	$\beta_1$	$\gamma_1$	$\lambda_2$	$\beta_2$	$\gamma_2$
One-spot model							
50293	radio	353	-78	22.3	-	-	-
	X-rays	362	-78	21.4	-	-	-
50321	radio	350	-83	32.7	-	-	-
	X-rays	359	-79	34.1	-	-	-
50349	radio	371	-84	30.5	-	-	-
	X-rays	345	-79	29.6	-	-	-
50377	radio	365	-79	28.9	-	-	-
	X-rays	337	-81	26.8	-	-	-
Two-equatorial-spot model							
50293	radio	340	0	9.5	86	0	5.1
	X-rays	335	0	7.5	57	0	6.1
50321	radio	323	0	14.1	96	0	10.9
	X-rays	318	0	15.5	78	0	11.6
50349	radio	316	0	11.4	80	0	10.7
	X-rays	313	0	11.8	57	0	9.3
50377	radio	353	0	13.5	111	0	8.4
	X-rays	304	0	9.9	58	0	7.8
Two-spot model							
50293	radio	335	-64	13.0	48	81	11.6
	X-rays	332	-65	12.9	57	-63	10.4
50321	radio	323	-73	26.4	104	67	13.9
	X-rays	326	-66	27.1	89	-18	10.9
50349	radio	361	-84	30.7	153	-50	2.4
	X-rays	360	-78	26.8	292	-17	11.9
50377	radio	338	-65	19.7	98	-18	8.9
	X-rays	317	-74	22.4	86	-59	10.1

### 5.2. The mechanism of flux ratio change of ARs

The area increase of the AR with time is due to the diffusion of its magnetic field (Fig. 8, top). The magnetic field in the photosphere is subjected to persistent large-scale flows and more rapidly evolving convective flows (supergranular and granular), which disperse the field (for more details see van Driel-Gesztelyi 1998 and references therein). We see that even the longest-living leading spot represented by the round-shaped positive polarity (white) concentration in Fig. 8 disappeared by September (the third analysed rotation). The initially intensive flaring also strongly decreased with the dispersion of the magnetic fields. A random walk diffusion by granular and supergranular motions and the differential rotation created the characteristic elongated double lobe magnetic field pattern of the aging AR. We observed chromospheric and coronal emission from all over the actual magnetic extension of the AR (c.f. the magnetic images with the He II images in Fig. 8). As the area of the AR was getting larger and the magnetic flux density was getting lower, so decreased the intensity of the emission from the related loops.

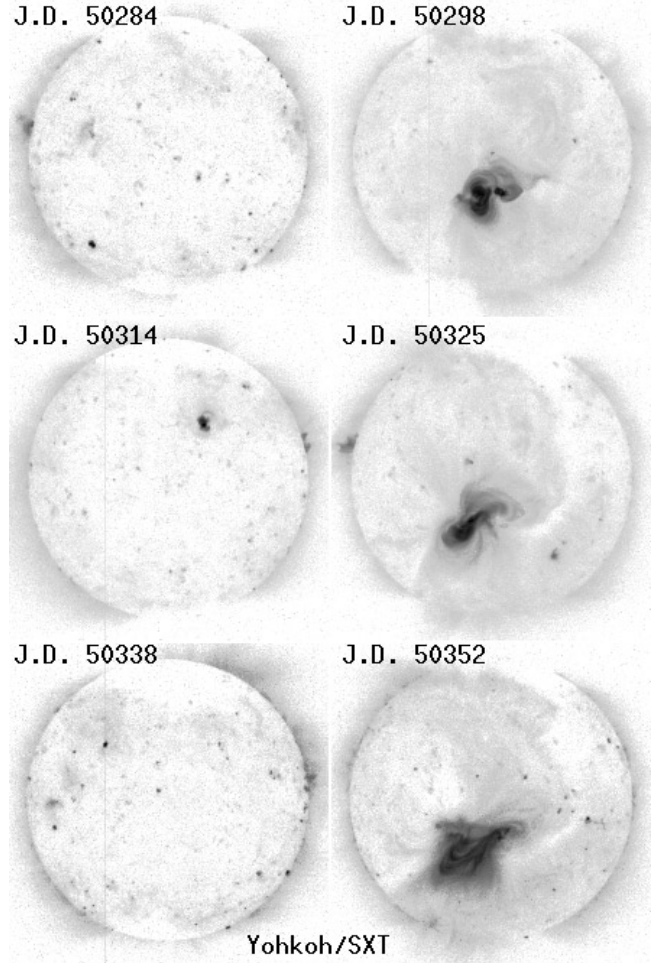


**Fig. 6.** Series of X-ray images of the Sun, made by the Yohkoh spacecraft. For better contrast, negative images are shown. Note the small AR in the middle panel of the left column.

Comparing the evolution of the coronal emission to the observations taken in the visual domain, the sense of changes is obviously the opposite, but the basic link between them is provided by the magnetic fields. As the area of the AR is increased by the magnetic diffusion, the facular area grows, thus providing more emission. Meantime, the area of the spots decrease, eventually they disappear. The lifetime of sunspots is proportional to their maximal area (Petrovay & van Driel-Gesztelyi 1997); the faculae survive the spots. As the spot/facula ratio decreases, first the temperature of the integrated emitting surface increases. However, later the growing facular region provides less and less emission, thus we slowly approach the spotless brightness and temperature of the star.

A stellar analogue for the flux ratio changes was given by O'Neal et al. (1998), who found spectroscopic evidence for changing spot temperatures within one rotation on the K sub-giant RS CVn type star II Peg, and also a correlation between the increased spot temperature and the stronger H $\alpha$  and Ca II emission. O'Neal et al. (1998) tried to explain their findings with changing spot sizes or variable umbra-penumbra ratios.

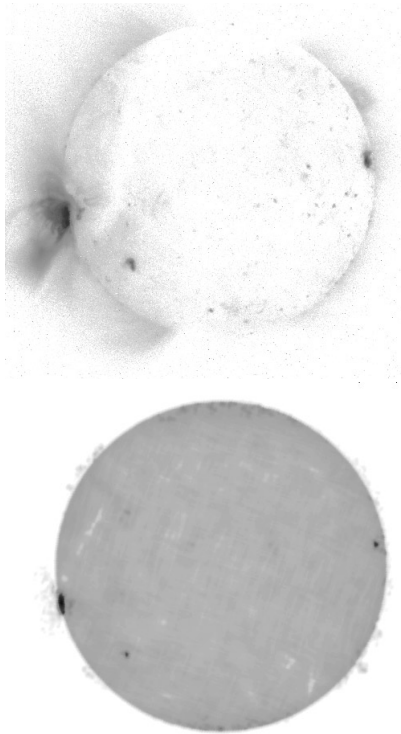


**Fig. 7.** Yohkoh X-ray and Nobeyama radio images of the Sun on 24 August, 1996. For an increased contrast, negative images are displayed. Note the two small ARs beside the main one. More explanation is in the text.

## 6. Conclusion

Comparing our spot modellings with the direct images of the Sun, we arrived to the following conclusions that could be important for understanding starspot modelling results:

- The modelled total area of the disturbed regions seems to be close to the reality (to the direct measurements), if the intensity of the undisturbed surface and flux ratio between that and the active region is well known. This fact means, that using careful long-term starspot modelling, the change of spottedness of stars can well be followed.
- The latitude of the spot(s) in the one- and two-spot models can be artificially high to account for the general (long-term) variability coupled with the shape of the light curve. This finding should be kept in mind when speaking about high latitude spots on stars: in those cases other, affirmative observations or theoretical aspects should be found.
- Modelling with two (or more) spots can reproduce both the deviations from the pure sinusoidal light curve and the change in the overall light level. When one of the resulting spot is small, it can account for short living spots at different places on the stellar surface, that modify the light curve, however, its coordinates are absolutely unstable (can be almost anywhere), especially in case of high inclination. This result gives a warning to adopt two active longitudes on

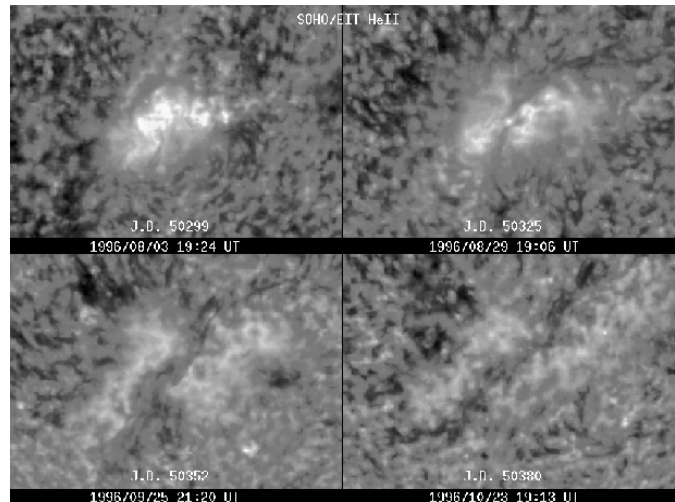
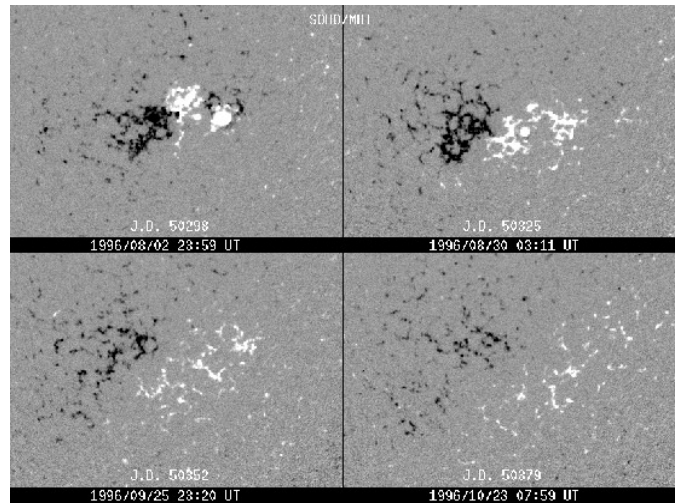


**Fig. 8.** SOHO/MDI magnetic maps (*top*) show the evolution of the magnetic field distribution of the remnant of the active region NOAA AR 7978 during four rotations around the time of consecutive central meridian passages of the AR. Note the diffusion of the magnetic field. SOHO/EIT He II ( $304 \text{ \AA}$ ) images (*bottom*) show that the emissivity decreases as the area of the AR increases.

- stars without other justification, such as e.g. clearly double-humped light curves that suggest two spots of similar size.
- Systematic changes in the solutions of spot sizes could hide changes in the flux ratio between the spot and the immaculate stellar surface.

*Acknowledgements.* We are indebted to P. Démoulin for fruitful discussions concerning flux ratio changes. Our referee, S. Catalano helped us with his suggestive comments. Thanks are due to D. Marik for his kind help in data handling. Financial supports from the Hungarian Government through OTKA T-019640, OTKA T-026165, OTKA F-019642, AKP 97-58 2,2 and the Hungarian-French Grant Balaton (F-42/96) are acknowledged. We thank the Yohkoh/SXT Team, the YoDac Data Center at MSSL, the SOHO/EIT and SOHO/MDI consortiums for images displayed in the figures. SOHO is a project of international cooperation between ESA and NASA. We made use of Nobeyama, DRAO, and GOES data archives.

## References

- Bartus J. 1996, *Occ. Techn. Notes at Konkoly Obs. No.1/96*
- Bopp B.W. & Evans D.S. 1973, MNRAS 164, 343
- Budding E. 1977, Ap&SS 48, 207
- Catalano S., Lanza A.F., Brekke P. et al. 1998, in: *Cool Stars, Stellar Systems and the Sun*, 10th Cool Star Workshop, Busto July 1997, Eds. R.A. Donahue and J.A. Bookbinder, in press
- Delaboudinière J.-P., Artzner G.E., Brunaud J. et al. 1995, Sol. Phys. 162, 291
- Hachenberg O. 1982, in: *Landolt-Börnstein Vol. 2b*, K. Schaifers & H.H. Voigt (eds.), Springer-Verlag Berlin-Heidelberg-New York, p. 105
- Hanaoka Y., Shibasaki K., Nishio M. et al. 1994, in: *New Look at the Sun with Emphasis on Advanced Observations of Coronal Dynamics and Flares*, Proc. Kofu Symposium, S. Enome & T. Hirayama (eds.), NRO Report No. 360, p. 35
- Harvey K.L., Hudson H.S. 1997, in: *Observational Plasma Astrophysics: Five Years of Yohkoh and Beyond*, T. Watanabe, T. Kosugi, A. C. Sterling (eds.), Kluwer, p. 315
- Hudson H.S., Labonte B.J., Sterling A.C., Watanabe T. 1997, in: *Observational Plasma Astrophysics: Five Years of Yohkoh and Beyond*, T. Watanabe, T. Kosugi, & A. C. Sterling (eds.), Kluwer, p. 237
- Kóvári Zs., Bartus J. 1997, A&A, 323, 801
- Nishio M., Nakajima H., Enome S. et al. 1994, in: *New Look at the Sun with Emphasis on Advanced Observations of Coronal Dynamics and Flares*, Proc. Kofu Symposium, S. Enome & T. Hirayama (eds.), NRO Report No. 360, p. 19
- O'Neal D., Saar S.H., Neff J.E. 1998, ApJ 501, L73
- Peres G., Orlando S., Reale F. et al. 1998, in: *Observational Plasma Astrophysics: Five Years of Yohkoh and Beyond*, T. Watanabe, T. Kosugi & A.C. Sterling (eds.), Kluwer, p. 29
- Petrovay K., van Driel-Gesztelyi L. 1997, Sol. Phys. 176, 249
- Press, W.H., Flannery B.P. Teukolsky S.A., Vetterling W.T. 1988, *Numerical Recipes in C*, Cambridge University Press
- Scherrer P.H., Bogart R.S., Bush R.I. et al. 1995, Sol. Phys. 162, 129
- Strassmeier K.G., Oláh K. 1992, A&A 259, 595
- Tapping K.F., Charrois D.P. 1994, Sol. Phys. 150, 305
- Tsuneta S., Acton L., Bruner M. et al. 1991, Sol. Phys. 136, 37
- van Driel-Gesztelyi L. 1998, in: *Three Dimensional Structure of Solar Active Regions*, Proc. 2nd ASPE, C. Alissandrakis & B. Schmieder (eds.), ASP Conf. Ser. 155, 202